Brain Advance Access published March 29, 2013

BRAIN
A JOURNAL OF NEUROLOGY

OPA1 loss of function affects *in vitro* neuronal maturation

Ambre M. Bertholet,[1] Aurélie M.E. Millet,[1] Oriane Guillermin,[1] Marlène Daloyau,[1] Noélie Davezac,[1] Marie-Christine Miquel[1,2,*] and Pascale Belenguer[1,*]

1 Université de Toulouse, Centre de Biologie du Développement, CNRS UMR5547/Université Paul Sabatier, Toulouse, France
2 UPMC Université Pierre et Marie Curie, Sorbonne Universités, Paris, France

*These authors contributed equally to this work.

Correspondence to: Pascale Belenguer
CNRS UMR 5547/Université Paul Sabatier,
Bât 4R3BB3,
118 route de Narbonne,
31062 Toulouse,
France
E-mail: pascale.belenguer@univ-tlse3.fr

Mitochondrial dynamics control the organelle's morphology, with fusion leading to the formation of elongated tubules and fission leading to isolated puncta, as well as mitochondrial functions. Recent reports have shown that disruptions of mitochondrial dynamics contribute to neurodegenerative diseases. Mutations of the inner membrane GTPase OPA1 are responsible for type 1 dominant optic atrophy, by mechanisms not fully understood. We show here that in rodent cortical primary neurons, downregulation of the OPA1 protein leads to fragmented mitochondria that become less abundant along the dendrites. Furthermore, this inhibition results in reduced expression of mitochondrial respiratory complexes as well as mitochondrial DNA, decreased mitochondrial membrane potential, and diminished reactive oxygen species levels. The onset of synaptogenesis was markedly impaired through reductions in pre- and postsynaptic structural protein expression and synapse numbers without first affecting the dendritic arborization. With longer time in culture, OPA1 extinction led to a major restriction of dendritic growth, together with reduction of synaptic proteins. Furthermore, in maturing neurons we observed a transitory increase in mitochondrial filament length, associated with marked changes in the expression levels of OPA1, which occurred at the onset of synaptogenesis simultaneously with transitory increase in reactive oxygen species levels and NRF2/NFE2L2 nuclear translocation. This observation suggests that mitochondrial hyperfilamentation acts upstream of a reactive oxygen species-dependent NRF2 transcriptional activity, possibly impacting neuronal maturation, such a process being impaired by insufficient amount of OPA1. Our findings suggest a new role for OPA1 in synaptic maturation and dendritic growth through maintenance of proper mitochondrial oxidative metabolism and distribution, highlighting the role of mitochondrial dynamics in neuronal functioning and providing insights into dominant optic atrophy pathogenesis, as OPA1 loss affecting neuronal maturation could lead to early synaptic dysfunction.

Keywords: OPA1; DOA; synaptic maturation; mitochondrial dynamics; ROS

Abbreviation: DOA = dominant optic atrophy

Received July 17, 2012. Revised December 21, 2012. Accepted January 25, 2013.

Introduction

The highly specialized nature and architecture of neurons presents a challenge for mitochondria, which must furnish energy and buffer calcium in remote parts of the cell and in specialized domains. Furthermore, the organelle must adapt to variations in neurotransmission activity. The importance of mitochondria in neurons is emphasized by the impaired mitochondrial function that occurs in numerous neurodegenerative diseases, such as Parkinson's disease and Alzheimer's disease (reviewed in Schon and Przedborski, 2011). Additionally, recent reports have suggested that not only perturbation of mitochondrial metabolism but also disruptions of mitochondrial dynamics, which control mitochondrial morphology, contribute to neurodegenerative diseases (Schon and Przedborski, 2011).

Mitochondrial morphology varies according to cell type and cellular context, ranging from an interconnected filamentous network to isolated spheres, depending both on the cytoskeleton, which controls mitochondrial distribution and motility (reviewed in Boldogh and Pon, 2007), and on recently discovered mitochondrial dynamics (reviewed in Westermann, 2010). This dynamic balance between fission and fusion of mitochondrial membranes depends on protein complexes conserved throughout evolution. Increasing fusion leads to interconnected mitochondrial filaments; increasing fission leads to isolated dot-like structures. Key proteins involved in fission are Dynamin-Related Protein 1 (DRP1), MFF1 and FIS1, while the mitofusins (MFN1 and MFN2) and OPA1 control fusion. The functional relevance of mitochondrial dynamics is emphasized both by its repercussions on such key processes as respiration, calcium homeostasis, reactive oxygen species production, apoptosis, and by its requirement during embryonic development (Westermann, 2010). Furthermore, while this process is ubiquitous, several data highlight the importance of mitochondrial dynamics in neurons. Conditional MFN2 and DRP1 knockouts in mice are indeed associated with defects in CNS neuronal development (Chen *et al*., 2007; Ishihara *et al*., 2009), and mutations of MFN2 and OPA1 are responsible for type 2 Charcot–Marie–Tooth peripheral neuropathy and type 1 dominant optic atrophy (DOA), respectively (Delettre *et al*., 2000; Zuchner *et al*., 2004).

Pathogenic OPA1 mutations account for ~60% of autosomal dominant optic atrophy, a common cause of inherited visual failure, with a frequency of 1:50 000 (reviewed in Amati-Bonneau *et al*., 2009). OPA1 is an ubiquitously expressed GTPase that is present in mitochondria as long and short isoforms generated by limited intra-mitochondrial proteolysis (reviewed in Landes *et al*., 2010). Both isoforms of OPA1 are localized in the intermembrane space and are primarily associated with the inner mitochondrial membrane. OPA1 plays a central role not only in the maintenance of mitochondrial morphology but also in protecting cells from apoptosis, the two functions being independent (Olichon *et al*., 2003, 2007; Cipolat *et al*., 2004; Frezza *et al*., 2006). OPA1 was also recently found to be involved in mitochondrial DNA maintenance (Elachouri *et al*., 2011). Most of the >200 different OPA1 mutations result in premature termination codons, with truncated messenger RNA that are unstable and degraded by nonsense-mediated messenger RNA degradation (Amati-Bonneau *et al*., 2009). The reduction in OPA1 protein levels is a major disease mechanism, and the importance of haploinsufficiency is further emphasized by rare families carrying a deletion of either the entire or most of the OPA1 open reading frame (Amati-Bonneau *et al*., 2009). Although optic nerve degeneration remains the defining feature of DOA, up to 20% of patients with OPA1 mutations also develop additional extraocular neurological complications (DOA+ syndrome), including deafness, ataxia, myopathy, peripheral neuropathy and progressive external ophthalmoplegia (Yu-Wai-Man *et al*., 2010). The extent to which inactivation of OPA1 functions contributes to DOA and DOA+ pathogenesis remains to be elucidated. Data on non-neuronal cell lines, such as HeLa cells, mouse embryonic fibroblasts and skin fibroblasts from patients with DOA or DOA+ suggest that impairment of mitochondrial morphology, functions and/or increased sensitivity to apoptosis could be involved (Landes *et al*., 2010). Because haploinsufficency is primarily responsible for DOA and as the effects of OPA1 inactivation are not restricted to retinal ganglionic cells, we addressed the question of the general impact of OPA1 inactivation in neurons by downregulating OPA1 in rat cortical neurons in primary culture.

We showed that downregulation of OPA1 leads to fragmented mitochondria that become less abundant along the dendrites. Furthermore, this inhibition results in reduced expression of mitochondrial respiratory complexes as well as mitochondrial DNA, decreased mitochondrial membrane potential, and diminished reactive oxygen species levels. Moreover, reduction of OPA1 protein leads to reduction of synaptic protein expression levels and synapse number, followed by drastic alterations of dendritic arborization. Altogether, these results suggest that lowering OPA1 protein levels, through alterations in oxidative metabolism exacerbated by a reduction in dendritic mitochondrial content, could primarily affect neuronal maturation leading to early neuronal dysfunctions. Interestingly, in maturing neurons we observed a transitory increase in mitochondrial filament length, associated with marked changes in the expression levels of OPA1, which occurred at the onset of synaptogenesis simultaneously to transitory increases in reactive oxygen species levels and NRF2/NFE2L2 nuclear translocation. This observation suggests that mitochondrial hyperfilamentation acts upstream of a reactive oxygen species-dependent NRF2 transcriptional activity, possibly impacting neuronal maturation, such a process being impaired by insufficient amount of OPA1.

Materials and methods

Primary culture and transfection

All animals ($n = 50$) in this study were ethically maintained and used. Embryos ($n = 400$) were removed at embryonic Day 17 from pregnant Wistar rats (Janvier) under intraperitoneal pentobarbitol (Sigma) anaesthesia. Cortices were dissected, enzymatically dissociated with papain (10 U/ml, Sigma), and plated on poly-D-lysine (0.1 mg/ml, Sigma) coated Petri disches with or without glass cover-slips. For each experiment, cortices from 8 to 12 embryos per rat are mixed. Experiments were reproduced three to eight times.

Cultures were grown in Neurobasal® (Eurobio) supplemented with B27 (Invitrogen), 2 mM glutamine, and 0.1% penicillin and

streptomycin (Gibco), 250 U/ml amphotericin (Invitrogen), 1 mM lactic acid (Sigma) at a density of 6×10^5 cells per cm^2.

Cells (5×10^6) were electroporated after dissociation using the Rat Neuron Nucleofector® Kit (AMAXA®, Lonza) using an optimized protocol for primary rat cortical neurons (http://bio.lonza.com/fileadmin/groups/marketing/Downloads/Protocols/Generated/Optimized_Protocol_101.pdf). Three micrograms of control luciferase-targeting (D-001210-02, control small interfering RNA) or OPA1-targeting (target sequence GAUUGUGCCUGACUUUAUA, small interfering RNA against OPA1) small interfering RNA (Dharmacon), with or without 3 μg MitoDSRed2 plasmid (Clontech) were used.

Using vectors expressing fluorescent pan-cellular (GFP) or mitochondrial (MitoDSRed2) proteins, we estimated after 72 h the efficiency of electroporation to be 37 ± 3% and 36 ± 4%, respectively ($n = 3$, 300 cells per condition). However, the efficiency of electroporation of the small interfering RNA OPA1, which we estimated at 6 days *in vitro* using a functional criterion (mitochondrial fragmentation), is much higher i.e. ~60% (Fig. 3C).

Viability of plated cortical cells was estimated using the Trypan blue exclusion assay. Neurons were incubated in the presence of 0.2% Trypan blue in PBS for 3 min. The number of viable cells, i.e. which exclude the dye, was estimated by counting under light microscope (Supplementary Fig. 1). Viability of untransfected cells was ~82% ($n = 3$, 300 cells per condition) from 2 days *in vitro* to 12 days *in vitro* (Supplementary Fig. 1A). Viability of transfected cells at 2 days *in vitro* was 81 ± 2% (Supplementary Fig. 1B) and was identical for control small interfering RNA and small interfering RNA against OPA1 until 12 days *in vitro* (Supplementary Fig. 1C) ($n = 3$, 300 cells per condition).

Measurement of reactive oxygen species and mitochondrial membrane potential

Reactive oxygen species levels were measured using the fluorescent dye 2′,7′-dichlorodihydrofluorescein diacetate (CM-H_2DCFDA, Molecular Probes). This dye passively diffuses into the cells, where its acetate groups are cleaved by intracellular esterases and its thiol-reactive chloromethyl group reacts with intracellular glutathione and other thiols. Subsequent oxidation yields a fluorescent adduct. Cortical cells were incubated (five dishes per condition, $n = 5$ independent experiments) with CM-H_2DCFDA at 4 μM for 30 min at 37°C in growth medium. Cells were then washed in cold PBS and scraped in cold water to be disrupted. Reactive oxygen species levels were measured (490 nm excitation, 520 nm emission) using a Wallac spectrofluorimeter (Perkin Elmer). Levels of fluorescence were standardized to protein levels that were estimated using a Lowry-based colorimetric assay (DC protein assay, Bio-Rad).

Mitochondrial membrane potential was measured using the cationic, voltage-sensitive dye 5,5′,6,6′-tetrachloro-1,1′,3,3′ tetraethylbenzimidazolylcarbocyanine iodide (JC-1, Invitrogen). The monomeric form of this dye has a green fluorescence, while at higher concentrations or potentials it forms red fluorescent J-aggregates. The ratio of red/green fluorescence is independent of mitochondrial shape, density or size, but depends on the membrane potential. Cortical cells were incubated (five dishes per condition, $n = 5$ independent experiments) with JC-1 at 2 μg/ml for 20 min at 37°C in growth medium. Cells were then washed and scraped in cold PBS. Ratio of red fluorescence (488 nm excitation, 590 nm emission) to green fluorescence (488 nm excitation and 525 nm emission) were quantified using a Wallac spectrofluorimeter (Perkin Elmer).

Immunocytochemistry

Cells were fixed with PBS containing 3.7% formaldehyde for 20 min, permeabilized for 15 min in PBS, 1% bovine serum albumin, 0.3% Triton™ X-100 and blocked for 1 h in PBS containing 5% normal goat serum, 3% bovine serum albumin, 0.5% Tween 20. Alternatively, methanol fixation (10 min, −20°C) was performed prior to nuclear NRF2 detection. Polyclonal or monoclonal antibodies against Map2, Beta 3 tubulin (both 1/1000, Sigma), NRF2 (Santa Cruz, 1/50), synapsin (1/800, Synaptic Systems), synaptophysin (1/500, Abcam), PSD95 (1/800, Millipore), DNA (1/50, Progen) and all five mitochondrial respiratory complexes (MitoProfile® Total OXPHOS 1/50, MitoSciences), were incubated overnight at 4°C in blocking solution. Cells were then incubated with appropriate Alexa-conjugated secondary antibodies (1/1000, Molecular Probes), labelled with 0.25 μg/ml Hoechst in PBS over 5 min, and mounted in Mowiol®. Immunolabelling was visualized under a fluorescence microscope (Nikon Eclipse 80i or SP2-Leica), and images were acquired using NIS-Element (Nikon Digital Sight DSU2 camera) or SP2-Leica software. Mitochondrial size was measured in the somatic/proximal part of dendrites using ImageJ software and confocal images (×63) (average of 1500 mitochondria per 35 neurons per time point, $n = 3$). Dendrite length, branching and number were measured for five to ten neurons per cover-slip (three cover-slips per condition, three to five independent experiments) using the NeuronJ add-on to ImageJ software (http://rsbweb.nih.gov/ij/) and digitized images (×100). Quantification of synaptic elements was automatically performed using the ImageJ software after intensity thresholding. Synapses were counted when pre- and post-synaptic markers co-localized (×100, 10 independent fields per well, three cover-slips per condition, $n = 3$ independent experiments). Mitochondrial area and number were measured using the ImageJ software and confocal images (×63) of 10 independent fields per cover-slip (three cover-slips per condition, total average of seven neurons, $n = 4$ independent experiments). Quantification of mitochondrial DNA was automatically performed using the Volocity® 3D Image Analysis Software after intensity thresholding and elimination of nuclear fluorescence. Cytoplasmic fluorescent dots were counted as mitochondrial DNA when they co-localized with mitochondria (×100, eight independent fields per cover-slip, two cover-slips per condition, 18 neurons per condition, $n = 3$ independent experiments).

Immunoblot

In all experiments but those shown in Fig. 1, cells were scraped and suspended in Laemmli sample buffer and directly loaded on a gel (similar cell number). For Fig. 1 experiment, protein concentration was measured (Bio-Rad), after protein extraction in lysis buffer (50 mM Tris-HCl pH 7.5, 0.25 M NaCl, 5 mM EDTA and EGTA, 1 mM dithiothreitol, 0.1% Triton™ X-100, 0.1% deoxycholate, 0.1% NP40 and a cocktail of proteases inhibitors from Boehringer), and 50 μg per time point (0 to 12 days *in vitro*) were loaded on gels. Proteins were subjected to SDS-PAGE and electroblotted onto nitrocellulose membranes. After blocking in Tris-buffered saline with 0.2% Tween and 5% dry low-fat milk, membranes were treated with various primary antibodies [anti-actin (1/10 000, Chemicon), anti-DRP1 (1/200, BD Biosciences), anti-HSP60 (LK2, 1/200, Sigma), anti-MFN1 (1/50, gift from M. Rojo, Bordeaux), anti-MFN2 (1/200, Abnova), anti-OPA1 (1/300, BD Biosciences), anti-PSD95 (1/800, Millipore), anti-synapsin (1/800, Synaptic Systems), anti-synaptophysin (1/500, Abcam), anti-MFF1 (1/500, Abacam)] overnight at 4°C in blocking buffer. Antibodies directed against subunits of the five respiratory complexes are listed in Supplementary Table 1. After enhanced chemiluminescent detection of

horseradish peroxidase-labelled secondary antibodies (1/10 000, Abcam), scanned photographic films were analysed using ImageJ software.

Statistical analysis

Most of the experiments were statistically treated with paired student's *t*-test because of the systematic comparison between control small interfering RNA and small interfering RNA against OPA1-treated cells (Figs 2–8, Supplementary Figs 4C, 6 and 7). The ratio of long over short mitochondria (Fig. 1C), the distribution (area and number) of mitochondria in control small interfering RNA or in small interfering RNA against OPA1 (Supplementary Fig. 8) were investigated using an ANOVA to compare all the groups (Bartlett's test for equal variance and Newman Keuls Multiple comparison post-test). Analysis of MFN1, MFN2, DRP1, MFF1, actin and HSP60 quantities over time in culture (Fig. 1A and E and Supplementary Fig. 4A and B) were carried out with a non-parametric test (Kruskal-Wallis and a Dunn's multiple comparison post-test). $*P < 0.05$, $**P < 0.01$, $***P < 0.001$.

Results

Mitochondrial dynamics is differentially regulated during neuronal maturation

To unravel the impact of OPA1 inactivation in neuronal cells, we used embryonic rat cortical neurons grown in primary culture, a well-known *in vitro* model for neuronal maturation (Brewer, 1995). Neuronal growth was assessed by MAP2 (Supplementary Fig. 2A) and beta 3 tubulin immunostaining (not shown), and synaptic maturation was visualized by immunodetection of the presynaptic vesicle protein synaptophysin. Synaptophysin expression started after 4 days *in vitro* and accumulated until 12 days *in vitro*, as detected *in situ* (Supplementary Fig. 2B) or by western blot (Fig. 1A).

Before manipulating OPA1, we first evaluated the mitochondrial morphology of rat cortical neurons. Confocal microscopy images of the neuronal mitochondrial network throughout maturation were obtained after immunostaining of the mitochondrial respiratory chain complexes (Fig. 1B). At all days *in vitro*, the neuronal mitochondriome was filamentous, with a mean mitochondrial length of ~1.2 μm and ~27% of round mitochondria with circularity (biggest length/smallest length) of 1. After morphometric analysis, we grouped mitochondria in one of two classes: short (0.3 to 2 μm) or long (2 to 10 μm), as a function of time in culture. The ratio of long versus short mitochondria was roughly constant during the first days *in vitro*, but exhibited a transitory 3-fold increase at 6 days *in vitro* owing to an increase in the long population, after which the ratio rapidly returned to earlier levels (Fig. 1C).

We next characterized the expression of OPA1 during neuronal maturation by western blot (Fig. 1A). The OPA1 protein is composed of five isoforms ('a'–'e') (Supplementary Fig. 3); only the main ones (i.e. the long form 'b' and the short form 'd') are detected here. Interestingly, the ratio of these OPA1 'b'/'d' isoforms reveals a continuous increase from 2 to 12 days *in vitro* due to a higher expression of OPA1 long form (Fig. 1D). We also measured the expression of other key proteins involved in mitochondrial dynamics. Whereas MFN2 protein levels remained constant, those of MFN1 decreased significantly from 6 to 12 days *in vitro* (Fig. 1E). Furthermore, although two isoforms of DRP1 were detected in dissociated neurons before plating (0 days *in vitro*), only the longer isoform was present later on (Fig. 1A). The levels of MFF1 did not significantly change during *in vitro* neuronal maturation (Supplementary Fig. 4A), as those of mitochondrial protein HSP60 (used as loading control) and actin (Supplementary Fig. 4B). Similar changes in the expression of key regulators of mitochondrial dynamics were observed *in vivo* during cortical development, as assessed by western blots from embryonic Days 17 and 20 embryos, as well as from post-natal or adult cortices (Fig. 1F).

Transitory increases in mitochondrial potential, reactive oxygen species and NRF2 nuclear translocation during neuronal maturation

Because mitochondrial morphology changes can affect the functions of the organelle, we followed the evolution of two main parameters, mitochondrial membrane potential and reactive oxygen species levels. Indeed, the transitory mitochondrial hyperfusion observed at 6 days *in vitro* (Fig. 1C) was accompanied by a statistically significant transient 63 ± 22% increase in mitochondrial membrane potential, measured by spectrofluorometry through the red/green fluorescence ratio of the voltage-sensitive dye JC-1 (Fig. 2A). Similarly, we detected a 42 ± 9% augmentation of reactive oxygen species levels specifically at 6 days *in vitro*, as assessed by spectrofluorometry using CM-H_2DCFDA (Fig. 2B). Interestingly, we observed a similar time course for the nuclear translocation of the redox-sensitive NRF2 transcription factor (Supplementary Fig. 5), with a 2-fold increase at 6 days *in vitro* (Fig. 2C). To analyse the causal link between reactive oxygen species levels and hyperfilamentation, we pretreated the cells with the antioxidant Trolox™. Whereas this treatment reduced reactive oxygen species levels by 50% (Fig. 2D), it did not affect mitochondrial morphology at 6 days *in vitro*, the organelles remaining hyperfilamentous (Fig. 2E).

OPA1 downregulation alters mitochondrial morphology in neurons

To investigate the impact of OPA1 inactivation in neurons, we downregulated the expression of the profusion protein by RNA interference. Cortical neurons were transfected with small interfering RNA against OPA1 or control small interfering RNA before plating.

At 6 days *in vitro*, western blot analysis using anti-OPA1 antibodies revealed an effective knockdown of OPA1 expression (61 ± 8%, Fig. 3A). The effect of small interfering RNA against OPA1 downregulation on mitochondrial morphology was analysed under a fluorescent microscope by counting the number of MAP2-labelled neurons with fragmented DsRed2-labelled mitochondria at 6 days *in vitro* (Fig. 3B). Neurons were considered bearing a mitochondrial fragmented phenotype when they

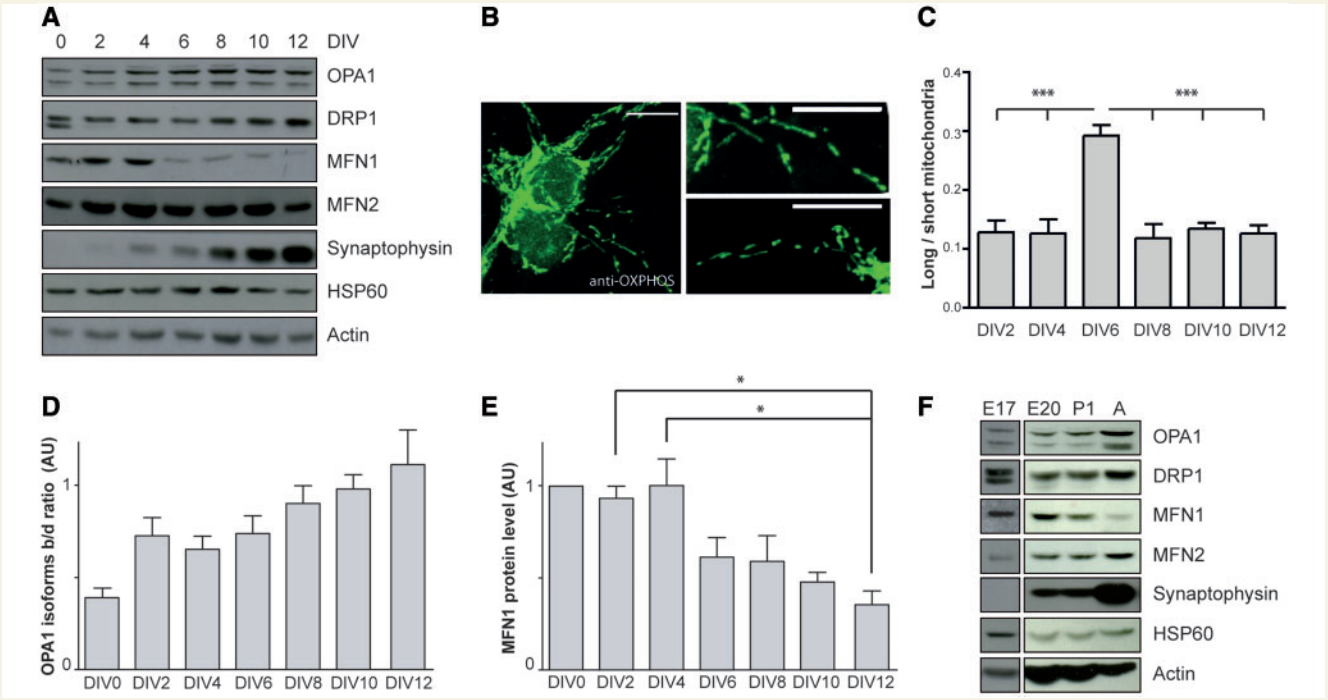

Figure 1 Mitochondrial dynamics during neuronal maturation. (**A**) Representative immunoblots showing the expression of various proteins from 0 day *in vitro* (i.e. Embryonic Day 17) to 12 days *in vitro*, with mitochondrial HSP60 and actin used as controls. (**B**) Confocal micrographs of neuronal mitochondria immunolabelled with respiratory chain complex antibodies (MitoProfile® Total OXPHOS) (*left*) showing long mitochondria in the *top right* and short mitochondria in the *bottom right*. Scale bar = 10 μm. (**C**) Quantification of mitochondrial size, in the somatic/proximal part of dendrites, over time in culture. Ratio of mean ± SEM of long (2 to 10 μM) versus short (0.3 to 2 μM) mitochondria per neurons from 2 to 12 days *in vitro* (average of 1500 mitochondria per 35 neurons per time point, $n = 3$). Statistical significance was determined by ANOVA. ***$P < 0.001$. (**D**) Histogram of the OPA1 'b'/'d' isoform ratio (AU = arbitrary units; mean ± SEM $n = 4$). Linear regression coefficient = 0.9947. (**E**) Histogram of the MFN1 protein levels over time, relative to HSP60 and normalized to values at 0 days *in vitro* (mean ± SEM, $n = 4$). Statistical significance was determined by the Kruskal-Wallis non-parametric test. *$P < 0.05$. (**F**) Representative immunoblots of the same proteins during development *in vivo* from protein extracts from cortices dissected at embryonic Days 17 (E17) and 20 (E20), at post-natal Day 1 (P1), and at the adult stage (A). DIV = days *in vitro*.

contained a majority of round and very short mitochondria (Fig. 3B). As expected, OPA1 downregulation led to a 6.5-fold increase in neurons with fragmented mitochondria, reaching 72 ± 9% of the total population (Fig. 3C). Morphometric analysis of mitochondria length in control small interfering RNA and small interfering RNA against OPA1 transfected neurons at 6 days *in vitro* showed that the mean mitochondria size decreased by 2-fold (Fig. 3D) and the percentage of round mitochondria (circularity = 1) increased by 2-fold upon OPA1 downregulation (Fig. 3E). No impact on OPA1 downregulation was observed on cell viability (Supplementary Fig. 1C), or on the spontaneous apoptotic neuronal death rate (Supplementary Fig. 1D).

OPA1 downregulation alters neuronal maturation

We analysed the possible consequences of the perturbation of mitochondrial morphology induced by OPA1 downregulation on the overall neuronal morphology, illustrated here by Map2 immunostaining (Fig. 3B). Morphometric analysis demonstrated that OPA1 downregulation did not modify dendritic arborization, in terms of either primary and secondary dendrite length or number at 6 days *in vitro* (Fig. 4A, Supplementary Fig. 6). We then addressed whether there would be an effect on synaptogenesis and found a decreased expression of both presynaptic (synaptophysin and synapsin) and postsynaptic (PSD95) markers (Fig. 5A), without significant change in the ratio of HSP60 and actin (used as loading control) levels (Supplementary Fig. 4C). Decreased amount of synaptic proteins was associated with a 45 ± 10% reduction in the number of synapses as estimated by co-localized immunostained punctua of pre- and postsynaptic markers (Fig. 5B).

With time in culture, up to 12 days *in vitro*, OPA1 downregulation (Supplementary Fig. 7) continued to negatively impact on both pre- and postsynaptic protein expression as estimated by western blot (Fig. 5C) or immunofluorescence microscopy (Fig. 5D, Supplementary Fig. 2B); their quantities staying nearly constant in small interfering RNA against OPA1-treated neurons as opposed to the expected increase in control neurons. The number of synapses decreased by 1.7- and 4-fold upon OPA1 downregulation at 9 and 12 days *in vitro*, respectively (Fig. 5E), while their respective quantities in the control situation increased by 1.7-fold from 9 to 12 days *in vitro*.

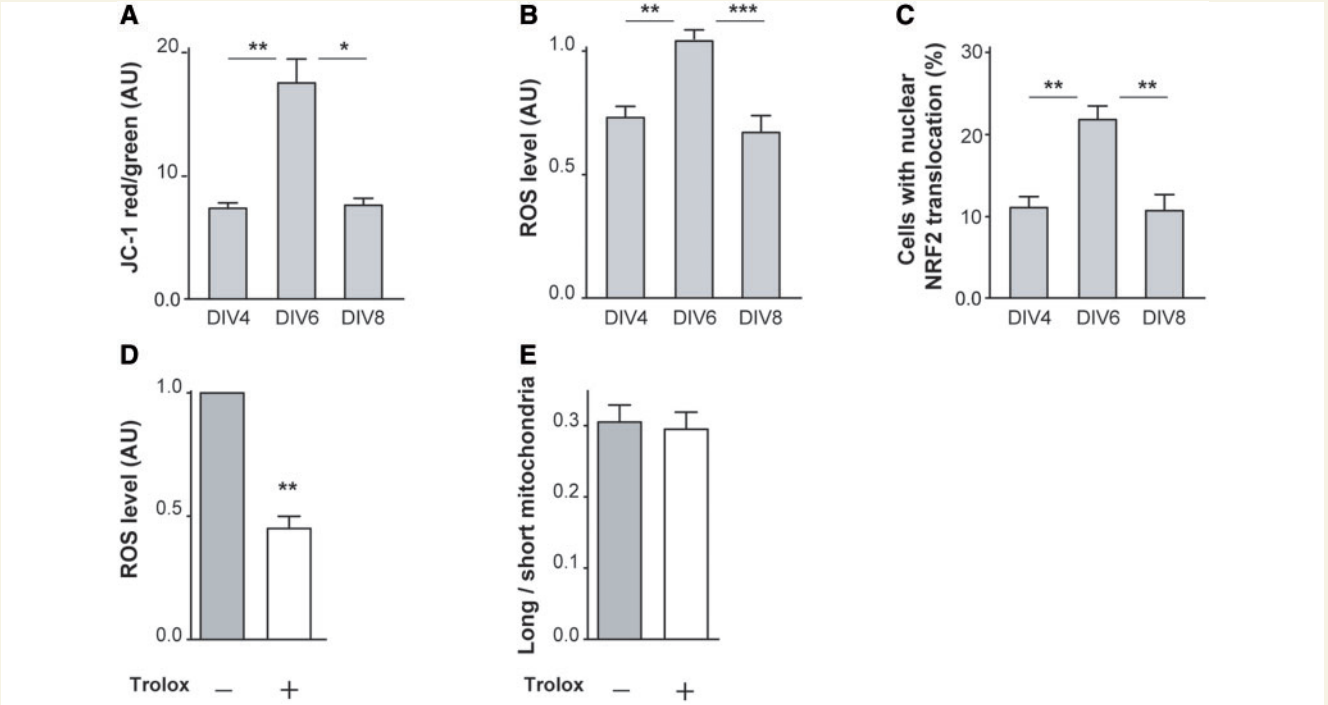

Figure 2 Mitochondrial membrane potential, reactive oxygen species level and NRF2 nuclear translocation during neuronal maturation. Quantification of JC-1-based mitochondrial membrane potential (590/525 nm ratio) (**A**) and of reactive oxygen species (ROS) level (**B**) at 4, 6 and 8 days *in vitro*. In both cases, bars represent the mean ± SEM of JC-1 ratio and CM-H_2DCFDA fluorescence values from one representative experiment (five culture dishes) out of five experiments (AU = arbitrary units). (**C**) Nuclear translocation of the transcription factor NRF2 estimated by immunostaining at 4, 6 and 8 days *in vitro* ($n = 4$). Effect of Trolox™ antioxidant treatment (100 μM for 6 h) at 6 days *in vitro* on (**D**) reactive oxygen species level (mean ± SEM, $n = 3$) and (**E**) on mitochondrial size [ratio of mean ± SEM of long (2 to 10 μM) versus short (0.3 to 2 μM) mitochondria (average of 1500 mitochondria per 35 neurons per time point, $n = 3$]. Statistical significance was determined by Student's *t*-test: $*P < 0.05$, $**P < 0.01$, $***P < 0.001$. DIV = days *in vitro*.

Interestingly, this prolonged synaptic decrease was then correlated to a reduced dendritic arborization (Fig. 4B–D), without significant impact on the spontaneous apoptotic neuronal death rate (Supplementary Fig. 1D). Starting at 9 days *in vitro*, dendritic morphometric analysis showed a progressive limitation of length of both primary and secondary dendrites up to 12 days *in vitro*, the population of smaller dendrites (<60 μm) being highly enriched in small interfering RNA against OPA1-treated neurons (Fig. 4B and C), while dendrite numbers were not affected (Supplementary Fig. 6). Dendritic growth is nevertheless observed but to a lesser extent than in control neurons, as attested by the lower percentages of longer processes. Therefore, we can conclude that impairing OPA1 function sequentially affects synaptogenesis, followed by dendritogenesis.

OPA1 downregulation alters mitochondrial distribution

We thus hypothesized that these synaptic and morphological changes may be linked to modifications of mitochondrial distribution and/or function. In control small interfering RNA and small interfering RNA against OPA1-treated neurons, filamentous and fragmented mitochondria, respectively, were detected along Map2-stained dendrites (Figs 3B, 4D and 6A). However, a quantitative analysis (Fig. 6B and C) showed that impairing OPA1 expression modified dendritic mitochondrial repartition. Mitochondria were measured (Fig. 6B) and counted (Fig. 6C) in contiguous 21 μm regions of interest in dendritic compartments, starting from the cell body. In control neurons, mitochondrial area per region of interest decreased rapidly, with the most proximal dendritic compartment containing almost 2.5-fold more mitochondrial surface than the distal compartments, the number of mitochondria being slightly lower in this compartment (Supplementary Fig. 8A). Upon OPA1 knockdown, mitochondria were still present in all dendritic compartments up to 170 μm from the soma; their area being unchanged along the dendrites (Supplementary Fig. 8B) and their number being slightly lower in distal part of the dendrites (Supplementary Fig. 8B). However, when compared with the control neuron values, the mitochondrial area per region of interest in small interfering RNA against OPA1-treated neurons was reduced along the dendrites, by ~9-fold in the more proximal part of the dendrites, and ~2-fold further along the dendrites (Fig. 4B); the number of mitochondria being significantly different only in the most proximal part of the neurites.

Because the overall mitochondrial mass was constant, as assessed by immunoblots of HSP60 (Supplementary Fig. 4C), our data suggested that OPA1 downregulation led, as soon as 6 days *in vitro*, to an increase in mitochondria in the soma and a reduction in the number of dendritic mitochondria, the fragmented organelles, however, being evenly distributed along the dendrites.

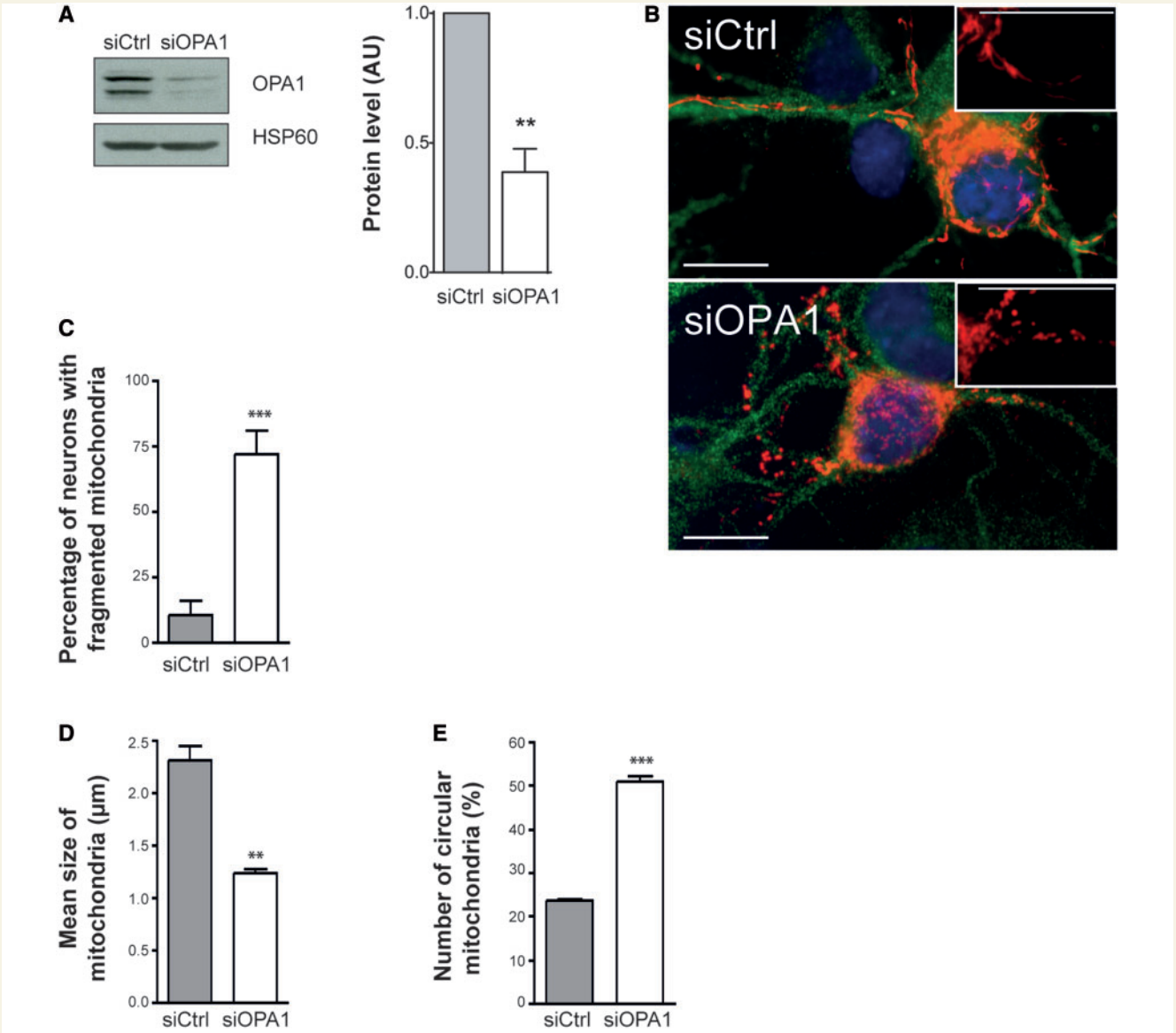

Figure 3 Effect of OPA1 downregulation on mitochondrial morphology. (**A**) Representative immunoblots (*left*) and histograms (*right*) representing at 6 days *in vitro* the expression of OPA1 protein relative to HSP60 levels after RNA interference, normalized to control values (AU = arbitrary units; mean ± SEM, $n = 6$). (**B**) Fluorescence micrographs (scale bars = 10 µm) of MitoDsRed2-labeled mitochondria (red) in Map2-immunostained neurons (green) transfected with control small interfering RNA (siCtrl; *top*) or small interfering RNA against OPA1 (siOPA1; *bottom*) at 6 days *in vitro*. Nuclei were Hoechst-labelled (blue). (**C**) Histogram representing the percentage of positive neurons for MitoDsRed2-transfected with control small interfering RNA or small interfering RNA against OPA1 with fragmented mitochondria at 6 days *in vitro* (mean ± SEM, average of 200 neurons per condition $n = 3$). (**D**) Histogram representing the mean size of MitoDsRed2-labelled mitochondria per neuron transfected with control small interfering RNA or small interfering RNA against OPA1 at 6 days *in vitro* (mean ± SEM, average of seven neurons per condition, $n = 4$). (**E**) Histogram representing the number of MitoDsRed2-labelled circular mitochondria per neuron transfected with control small interfering RNA or small interfering RNA against OPA1 at 6 days *in vitro* (mean ± SEM, average of seven neurons, $n = 4$ per condition). Statistical significance between small interfering RNA against OPA1 and control small interfering RNA-treated neurons was determined by Student's *t*-test: $^{**}P < 0.01$, $^{***}P < 0.001$.

OPA1 downregulation alters mitochondrial functioning

Following our hypothesis, we tested the effect of OPA1 knockdown on mitochondrial energetics. Mitochondrial membrane potential in cortical neurons transfected with OPA1-targeting or control small interfering RNA was estimated on 6 days *in vitro* by spectrofluorometry using the voltage-sensitive dye JC-1. The ratio of red to green fluorescence revealed a 25 ± 3% decrease in mitochondrial membrane potential of OPA1-depleted cells (Fig. 7A), which could reflect a reduced respiratory rate. Accordingly, a 22 ± 7% decrease in reactive oxygen species

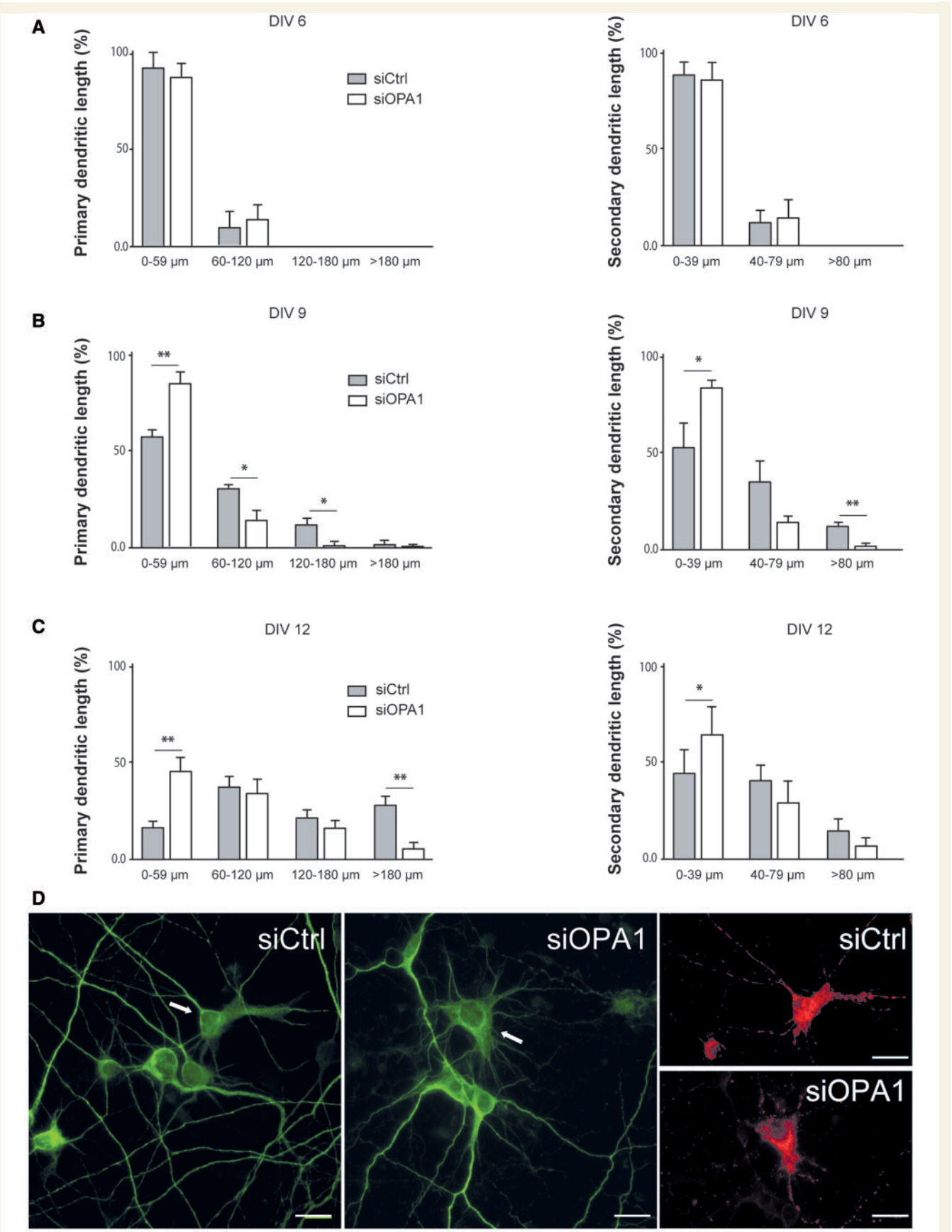

Figure 4 Effect of OPA1 downregulation on dendritic arborization. Histograms representing the quantification of Map2-immunostained primary (*left*) and secondary (*right*) dendrites length at 6 days *in vitro* (**A**), 9 days *in vitro* (**B**) and 12 days *in vitro* (**C**) after OPA1 downregulation. Bars represent the percentage of neurons with dendrites per class length (mean ± SEM, average of 30 neurons per

(continued)

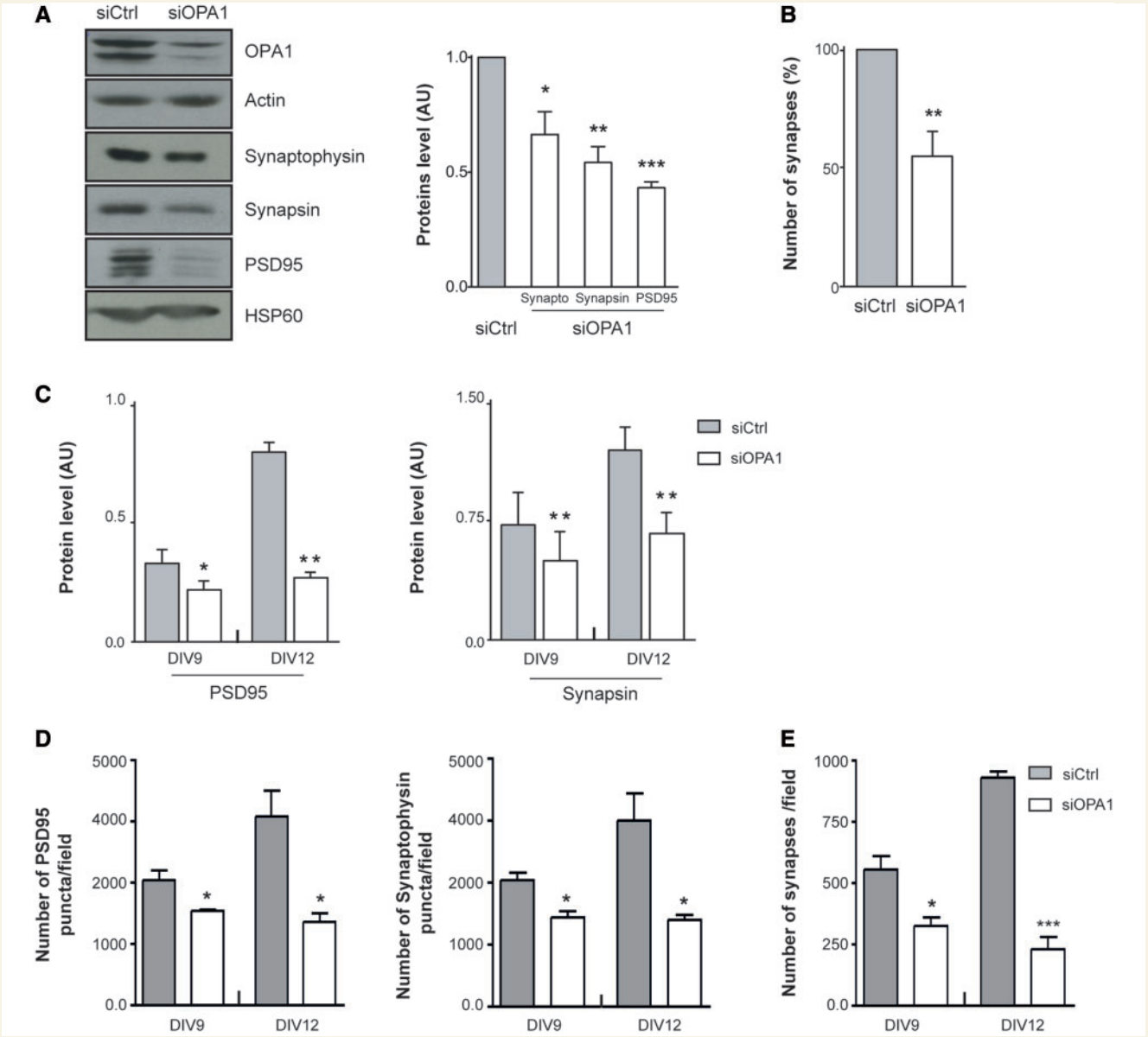

Figure 5 Effect of OPA1 downregulation on synaptic proteins. (**A**) Representative immunoblot showing the effect of OPA1 knockdown on the expression of synaptic proteins at 6 days *in vitro* (*left*), with the histogram representing the expression of the synaptic proteins relative to actin normalized to control values (*right*). (**B**) Histograms representing the quantification of synapses at 6 days *in vitro* determined by the number of co-localized presynaptic and postsynaptic immunostained markers, normalized to control values (AU = arbitrary units; mean ± SEM, $n = 3$). (**C**) Histograms representing the impact of OPA1 downregulation on the quantities estimated by western blot of PSD95 (post-synaptic marker, *left*) and synapsin (presynaptic marker, *right*) at 9 and 12 days *in vitro* relative to actin (mean ± SEM, $n = 4$). (**D**) Histograms representing the impact of OPA1 downregulation on the quantities, estimated by immunofluorescence microscopy, of PSD95 (*left*) and synatophysin (presynaptic marker, *right*) at 9 and 12 days *in vitro*. Bars represent the numbers of pre- or postsynaptic puncta per field (mean ± SEM, $n = 3$). (**E**) Histograms representing the quantification of synapses at 9 and 12 days *in vitro* determined by the number of co-localized pre- and postsynaptic immunostained puncta per field (mean ± SEM, $n = 3$). Statistical significance between small interfering RNA against OPA1 (siOPA1) and control small interfering RNA (siCtrl)-treated neurons was determined by Student's *t*-test: $*P < 0.05$, $**P < 0.01$, $***P < 0.001$. DIV = days *in vitro*.

Figure 4 Continued
condition, $n = 3$). Statistical significance between small interfering RNA against OPA1 (siOPA1) and control small interfering RNA (siCtrl)-treated neurons was determined by Student's *t*-test: $*P < 0.05$, $**P < 0.01$. (**D**) Representative fluorescence micrographs of 12 days *in vitro* Map2-stained neurons transfected with control small interfering RNA (*left*) and small interfering RNA against OPA1 (*centre*). Representative neurons (white arrow) are shown in the right panels to show the mitoDsRed2-labelled mitochondria. Scale bars = 10 µm. DIV = days *in vitro*.

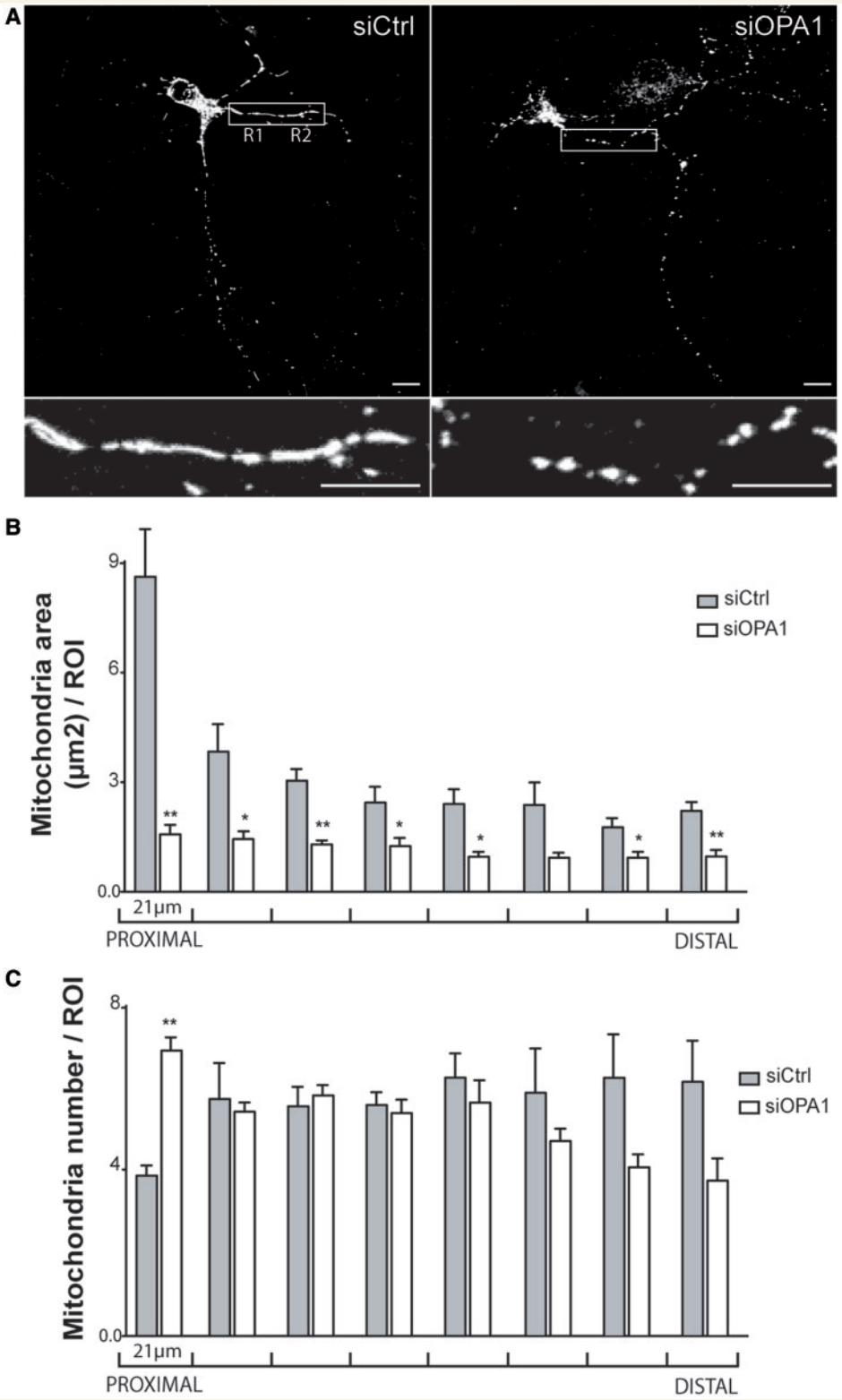

Figure 6 Effect of OPA1 downregulation on mitochondrial distribution in dendrites. (**A**) Fluorescence micrographs of MitoDsRed2-labelled mitochondria in dendrites. Magnified area in the bottom inserts representing rectangles encompassing two adjacent regions of interest (R1, R2) in the *upper* panels, show the long mitochondria (control small interfering RNA, *left*) versus the short ones (small interfering RNA against OPA1, *right*). Scale bars = 10 µm. (**B**) Histograms representing the mean mitochondrial area in eight dendritic regions of interest (ROIs, 21 µm long and 5 µm large segments) starting from the most proximal region (mean ± SEM, average of seven neurons, $n = 4$). (**C**) Histogram representing the number of mitochondria in each region of interest (mean ± SEM, average of seven neurons, $n = 4$). Statistical significance between small interfering RNA against OPA1 (siOPA1) and control small interfering RNA (siCtrl)-treated neurons was determined by Student's *t*-test: $*P < 0.05$, $**P < 0.01$.

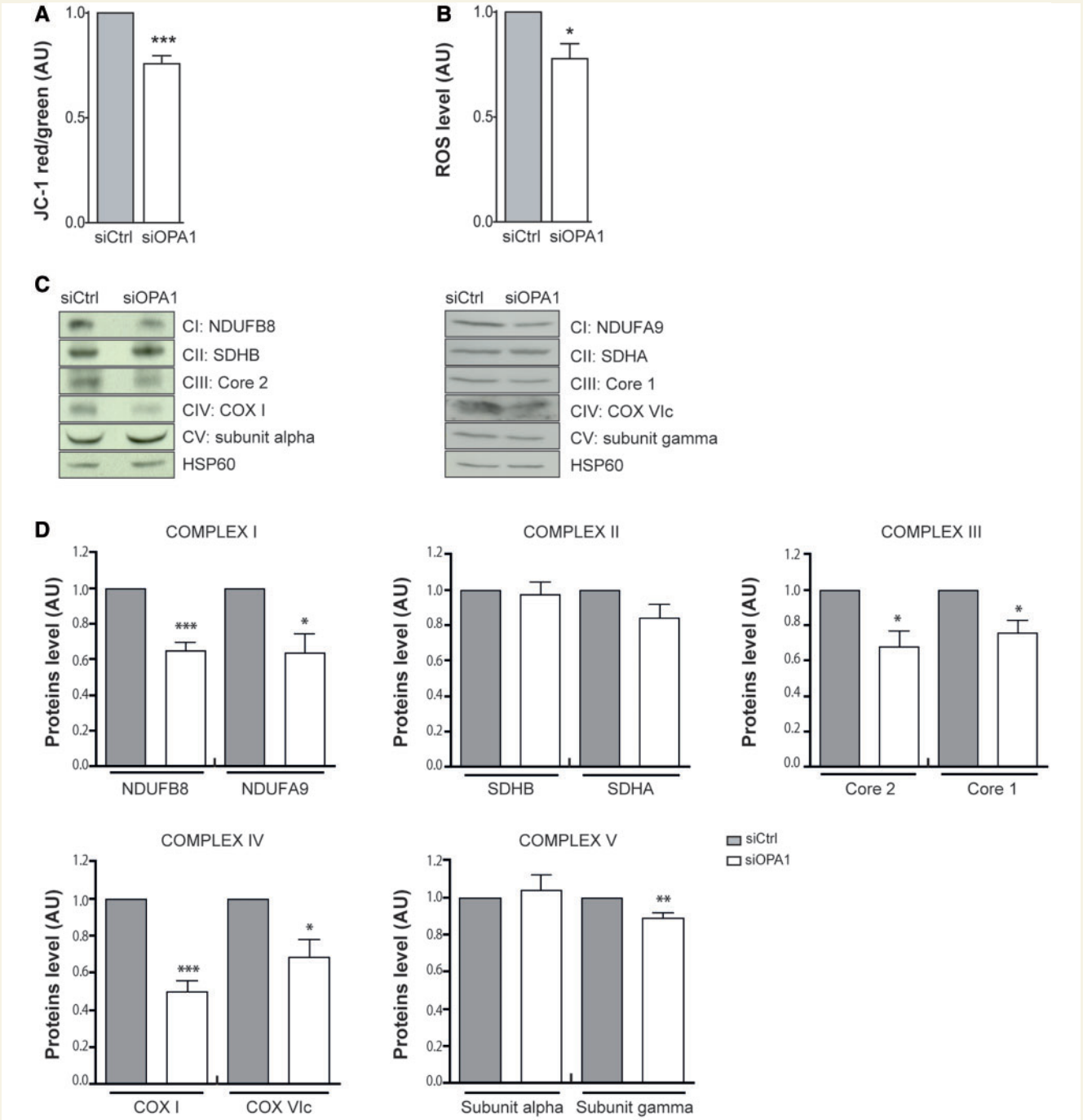

Figure 7 Effect of OPA1 downregulation on mitochondrial functions. Quantification of JC-1-based mitochondrial membrane potential (590/525 nm ratio) (**A**) and neuronal reactive oxygen species (ROS) level (**B**) upon OPA1 knockdown, normalized to control values (mean ± SEM, $n = 6$). (**C**) Representative immunoblot showing the effect of OPA1 knockdown on the levels of two subunits of the five mitochondrial respiratory protein complexes: NDUFB8 and NDUFA9 (Complex I, CI), SDHA and SDHB (Complex II, CII), Core 1 and Core 2 subunits (Complex III, CIII), COX1 and COXVIc subunits (Complex IV, CIV) and ATP5 subunits alpha and gamma (Complex V, CV). (**D**) Histogram representing the expression levels of the complexes relative to HSP60 levels and normalized to control values (mean ± SEM, $n = 6$). Statistical significance between small interfering RNA against OPA1 (siOPA1) and control small interfering RNA (siCtrl)-treated neurons was determined by Student's *t*-test: $^{*}P < 0.05$, $^{***}P < 0.001$.

levels was measured under these conditions (Fig. 7B). The decrease in mitochondrial membrane potential may have been due to reduced levels of mitochondrial respiratory chain complexes leading to decreased respiration. Indeed, western blot analysis of OPA1-depleted cells showed lower levels of two representative subunits of Complexes I, III and IV (Fig. 7C and D). In small interfering RNA against OPA1 transfected neurons the levels of NDUFB8 and NDUFD9 (Complex I) were 65 ± 5% and 64 ± 11%

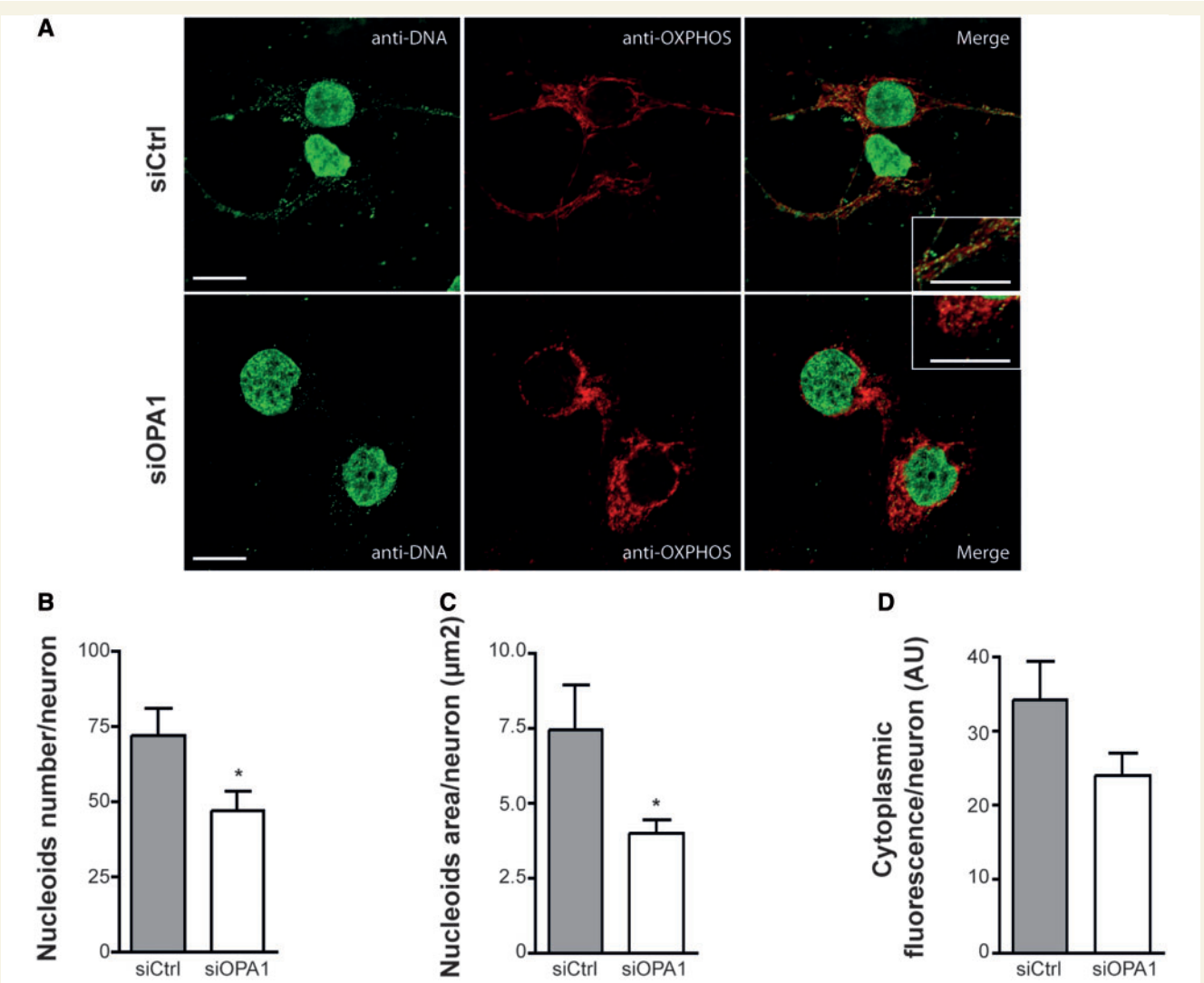

Figure 8 Effect of OPA1 downregulation on mitochondrial DNA. (**A**) Fluorescence micrographs of neurons transfected by control small interfering RNA (siCtrl) or small interfering RNA against OPA1 (siOPA1) at 6 days *in vitro*. Scale bars = 10 µm. Immunolabelling of mitochondria (red) and of DNA (green) were performed using anti-OXPHOS and anti-DNA antibodies, respectively. (**B**) Histograms representing the number of cytoplasmic green fluorescent dots, which co-localized with red fluorescence, per neurons in control small interfering RNA and small interfering RNA against OPA1 transfected neurons (mean ± SEM, 18 neurons per condition $n = 3$). (**C**) Histogram representing the total area of cytoplasmic green fluorescent per neuron in control small interfering RNA and small interfering RNA against OPA1-transfected neurons (mean ± SEM, 18 neurons per condition, $n = 3$). (**D**) Histograms representing the total fluorescence quantity of cytoplasmic green fluorescent per neurons in control small interfering RNA and small interfering RNA against OPA1-transfected neurons (mean ± SEM, 18 neurons per condition, $n = 3$). Statistical significance between small interfering RNA against OPA1 and control small interfering RNA-treated neurons was determined by Student's *t*-test: $^*P < 0.05$.

of the control, respectively; Core 2 and Core 1 subunit (Complex III) 68 ± 9% and 75 ± 7%, respectively; and COX1 and COXVIc subunit (Complex IV) 50 ± 6% and 68 ± 10%, respectively. No significant change was noticed for SDHA and B (Complex II), while the levels of the two subunits from Complex V were not significantly affected (α subunit) or only slightly decreased (γ subunit).

The decreased levels of mitochondrial DNA-encoded COX1 subunit prompted us to investigate if OPA1 downregulation led to mitochondrial DNA depletion in neurons, as it was previously described in non-neuronal cells (Elachouri *et al*. 2011). Mitochondrial DNA was evaluated by immunofluorescence microscopy using anti-DNA antibodies (Fig. 8). In control neurons green fluorescent dots, which correspond to mitochondrial DNA nucleoids, appeared evenly distributed within the mitochondrial network (Fig. 8A). At 6 days *in vitro*, downregulation of OPA1 led to a decreased number of mitochondrial DNA nucleoids (47 ± 6) when compared with control neurons (72 ± 9) (Fig. 8B), without major perturbations of their distribution (Fig. 8A). The total nucleoids area per neuron decreased in the same proportion in small interfering RNA against OPA1-treated neurons (7.4 ± 9 and 4.7 ± 0.6 in control small interfering RNA

and small interfering RNA against OPA1 cells, respectively, Fig. 8B), suggesting that no major alteration of nucleoid morphology occurred. Finally, total green cytoplasmic fluorescence diminished in small interfering RNA against OPA1 cells in the same proportion (34 ± 5 and 24 ± 3 in control small interfering RNA and small interfering RNA against OPA1-treated neurons, respectively), indicating that the total quantity of mitochondrial DNA is diminished (Fig. 8D).

Discussion

A growing body of evidence implicates mitochondrial dynamics in neurodegenerative diseases (Chen and Chan, 2009). Furthermore, links emerge between mitochondrial dynamics and neuronal physiology, particularly in terms of the reciprocal regulation of synapses and mitochondria (Li *et al*., 2004; Verstreken *et al*., 2005). On the other hand, few studies have focused on neuronal maturation, and are mainly concentrated on DRP1, which promotes mitochondrial fission (Li *et al*., 2008). We show here that establishment of a transitory hyperfilamentous mitochondrial network is crucial for synaptic maturation *in vitro*, and that this process is impaired by downregulation of the fusogenic OPA1 protein through alterations in oxidative metabolism exacerbated by a reduction in dendritic mitochondrial content. This results in reduced dendritic growth and synaptogenesis that could be related to impaired synaptic plasticity in adulthood associated with neurodegenerative diseases, and thus could participate in the aetiology of DOA.

Investigating the evolution of mitochondrial morphology during neuronal maturation in primary culture, we show that the mitochondriome of cortical neurons is filamentous, in line with previous reports (Chang and Reynolds, 2006; Uo *et al*., 2009; Voccoli and Colombaioni, 2009). In mature primary neuronal cells, mitochondrial size has been reported to increase by 20% compared with immature cells (Chang and Reynolds, 2006). During the course of neuronal maturation *in vitro*, our results demonstrate a transitory mitochondrial hyperfilamentation, mitochondrial size increasing at 6 days *in vitro* and decreasing thereafter to initial levels. This early transitory hyperfilamentation correlates with expression changes, *in vitro*, of the fission and fusion proteins that control mitochondrial morphology. The long form of the profission protein DRP1 was present at all days *in vitro* in culture and during development, while the short isoform was only present at the embryonic Day 17 stage. This pattern might be related to differential messenger RNA splicing, as cortical neurons have been reported to express several splice variants of DRP1, including a neuron-specific isoform that incorporates exon 3 (Uo *et al*., 2009), although nothing is known about their respective functions. Mitofusins behave differently during maturation, with MFN1 disappearing at 6 days *in vitro*, and after post-natal Day 1 *in vivo*, while MFN2 levels remain constant in both cases. Meanwhile, the ratio of the long fusogenic OPA1 isoform (Ishihara *et al*., 2006) over the short 'd' isoform continuously increased from 2–12 days *in vitro*. Because the fusogenic action of OPA1 depends critically on MFN1 (Cipolat *et al*., 2004), the filamentation process should be controlled by the OPA1/MFN1 ratio. Given the concomitant increase in the expression of the OPA1 long isoform and decrease in the expression of MFN1 at 6 days *in vitro*, this ratio could be responsible for the transient nature of this hyperfilamentation.

The general assumption is that longer filaments are beneficial for mitochondrial energy supplies, while fragmented mitochondria are more suitable for transport (reviewed in Westermann, 2012). Increase in mitochondrial filamentation has been shown to precede differentiation in immortalized neuroblasts (Voccoli and Colombaioni, 2009), as well as in myoblasts (De Palma *et al*., 2010) and in embryonic stem cells (Wilkerson and Sankar, 2011), suggesting a broader biological significance of this phenomenon. Therefore, the transitory increase in mitochondrial filamentation that we observed at 6 days *in vitro*, simultaneously with the onset of synaptophysin expression, could be a specific requirement of this stage of maturation, with mitochondria later fragmenting for transportation to remote parts of mature neurons. Interestingly, seminal work by Li *et al*. (2004) demonstrated that the number of mitochondria within dendritic protrusions increased during the active period of synaptogenesis and spine development in culture, together with local mitochondrial branching and filamentation. Furthermore, a creatinine-dependent increase in mitochondrial membrane potential has been reported to lead to an increase in the density of spines and synapses (Li *et al*., 2004), and ATP-dependent augmentation of synaptic activity is correlated with an increase in dendritic mitochondrial size (Chang *et al*., 2006). Reciprocally, impairing mitochondrial function with carbonyl cyanide *m*-chlorophenyl hydrazone has been reported to lead to neuritic retraction through mitochondrial membrane potential drop and fragmentation (Voccoli and Colombaioni, 2009), while the increase in oxidative metabolism that accompanies mitochondrial elongation seemed to be required for stem cell differentiation (Chung *et al*., 2007; Mandal *et al*., 2011; Wilkerson and Sankar, 2011). In line with these reports, both mitochondrial hyperfilamentation as well as synaptic marker expression and synapse number are impaired in OPA1-depleted cells, together with mitochondrial functioning (see below).

Recent work demonstrates that reactive oxygen species, which are frequently viewed as toxic molecules, play a crucial role in signalling pathways (Hamanaka and Chandel, 2010). The modest transitory increase in reactive oxygen species levels at 6 days *in vitro*, which we identified at the onset of synaptogenesis, may impinge on cell signalling, an idea in line with previous studies reporting increased reactive oxygen species levels during neuronal differentiation (Tsatmali *et al*., 2005). At this same early stage of maturation, we report a transitory increase in the nuclear translocation of the transcription factor NRF2, depletion of which was recently shown to delay *in vitro* neuronal differentiation (Zhao *et al*., 2009). Furthermore, antioxidant treatment at 6 days *in vitro* reduced reactive oxygen species levels, but did not interfere with the transitory hyperfilamentation, indicating that the observed increase in reactive oxygen species levels is downstream of the increase in mitochondrial size. Altogether, our findings suggest a transient requirement for mitochondrial hyperfilamentation during neuronal maturation leading to reactive oxygen species-dependent NRF2 signalling. Thus, as has been suggested for embryonic stem cells (Mandal *et al*., 2011), during early neuronal maturation, mitochondria may trigger specific retrograde signals,

including activation of transcription factors, that could travel to the nucleus and modulate the transcription of specific target genes.

Interfering RNA-mediated knockdown of OPA1, which led to a reduced expression of pre- and postsynaptic marker proteins and a decrease in synapse number as early as 6 days *in vitro*, had no impact on neuronal dendritic arborization (dendrite length and branching), hence on neuritogenesis at that stage. However, at 9 days *in vitro* and up to 12 days *in vitro*, dendritic growth became affected, and synaptic protein expression remained low. This suggests a new consequence of OPA1 extinction in neuronal maturation, first affecting synaptic maturation and later dendritic growth.

Deleterious effects of the profusion OPA1 loss of function on synapses and dendrites development could be expected given the crucial role of DRP1 and mitochondrial fission during the formation and maintenance of synapses and dendritogenesis (Supplementary Table 2). Inhibiting DRP1 in primary hippocampal neurons reduced dendritic mitochondrial content and led to a loss of synapses and dendritic spines whereas its overexpression increased dendritic mitochondrial content and enhanced the number and plasticity of spines and synapses (Li *et al*., 2004, 2008; Wang *et al*., 2009). However, controversial data have been reported by Dickey and Strack (2011), whose study of the opposing roles of enzymatic DRP1 inactivation/activation by phosphorylation/dephosphorylation in regulating neuronal development in hippocampal primary neurons led them to conclude that dendritic mitochondrial content and synapse number appeared negatively correlated (Dickey and Strack, 2011). Nonetheless, primary forebrain DRP1$^{-/-}$ neurons show both defective synapses and decreased numbers of neurites (Ishihara *et al*., 2009).

Several studies have demonstrated that DRP1 extinction perturbs synaptic development by drastically impairing the trafficking of mitochondria to neuronal processes (Li *et al*., 2004; Verstreken *et al*., 2005). On the other hand, we show here that mitochondrial fragmentation owing to impaired fusion resulted in a uniformly decreased mitochondrial occupancy in dendrites, in agreement with previous results obtained in transfected hippocampal neurons (Wang *et al*., 2009).

Overall, our data suggest that the impact of OPA1 knockdown on synaptogenesis and dendritogenesis occurs through disruption of mitochondrial oxidative metabolism, exacerbated by the reduction in mitochondria content. Indeed, we found that OPA1 knockdown led to reduced protein levels of the respiratory chain Complexes I, III and IV, which could be due to cristae disorganization (Olichon *et al*., 2003) impacting the stability and integrity of membrane-bound respiratory complexes or supra-complexes. Therefore, OPA1 could be suggested to be important for supra-complex formation or stabilization, structures known to optimize the respiratory complex activity and consequently ATP production (Lenaz and Genova, 2009). Alternatively, loss of mitochondrial DNA, which encodes part of Complexes I, III and IV would lead to the same results. We indeed showed that downregulation of OPA1 induced mitochondrial DNA depletion in neurons as previously reported in HeLa cells (Elachouri *et al*., 2011). Reduction of respiration was previously reported in OPA1-depleted non-neuronal cells, as well as in fibroblasts from patients with DOA bearing OPA1 mutations (Landes *et al*., 2010). This phenotype also applies to cortical neurons because OPA1 knockdown led to a decrease in mitochondrial membrane potential concomitant with a decrease in reactive oxygen species levels.

Finally, our findings suggest that OPA1 is required for proper mitochondrial functioning when energy needs are enhanced, e.g. for the formation and/or maintenance of synapses, and on dendritic growth, which mutually impact on each other. Our data offer new insights into both the impact of mitochondrial dynamics on CNS neuronal functioning, and the pathological processes leading to DOA. The first effect of OPA1 downregulation that we observed in cultured primary neurons is the decrease of the number of synapses that could be attributed to a reduction of the quantity of synaptic markers since both are decreased to the same extent at 9 days *in vitro* (reduction of ~1.7 and ~1.4-fold in small interfering RNA against OPA1 versus control small interfering RNA, respectively). Later, in mature neurons (12 days *in vitro*) the levels of synapses are more affected than those of synaptic markers (reduction of ~4 and ~2-fold in small interfering RNA against OPA1 versus control small interfering RNA, respectively), suggesting that maintenance of synapses is also affected. Early synaptic alterations are hallmarks of numerous neurodegenerative diseases, such as Alzheimer's disease, an age-related neurodegenerative process (Terry *et al*., 1991; Masliah *et al*., 2001). Similarly, early synaptic defects observed in Alzheimer's disease were recently associated with mitochondrial dysfunctions (Lee *et al*., 2012). Thus in DOA, an insufficient amount of OPA1 could reduce synapse formation in developing retinal ganglionic cells and induce, in time and/or under stressful conditions such as light exposition, more important synaptic defects resulting in retinal ganglionic cell degeneration. Accordingly, Williams *et al*. (2012) reported a marked reduction in retinal ganglionic cell synaptic connectivity in a DOA mouse model. In this mouse line, synaptic defects are accompanied by retinal ganglionic cell dendritic pruning, which preceded the onset of visual loss and structural changes in the optic nerve (Williams *et al*., 2010).

In conclusion, unravelling the role of OPA1-dependent mitochondrial dynamics on neuronal maturation and function will illuminate the physiopathological mechanisms underlying DOA and probably other neurodegenerative diseases. Such mechanistic details could give rise to long-awaited therapeutic solutions. In line with the current emerging hypothesis that impairment of mitochondrial dynamics is an early event in most neurodegenerative pathologies, playing a pivotal role in neuronal plasticity dysfunction, our findings may help to define targets that precede further cytotoxic phenomena.

Acknowledgements

We thank Nicolas Heck for helping with ImageJ macro encoding, Manuel Rojo for the gift of anti-MFN1 antibodies, Géraldine hoffer for sharing her expertise in primary neuronal culture, Alain Roulet for helping with statistical analyses and Brice Ronsin for helping with Velocity macro encoding and technical assistance in confocal analysis on the Toulouse RIO imaging plataform. We thank Vincent Setola, Jean-Michel Peyrin, Valérie Mils, Laëtitia

Arnauné and Didier Miquel-Vilette for critical reading of the manuscript and thoughtful discussions.

Funding

This project was supported by grants from the Centre National de la Recherche Scientifique, the Université Paul Sabatier, Rétina-France, the Association Française contre les Myopathies, the Union Nationale Des Aveugles et Déficients Visuels, 'Gueules Cassées' and the Association contre les Maladies Mitochondriales. A.B. was funded by the French Ministry for Research and Education and Rétina-France for PhD studies.

Supplementary material

Supplementary material is available at *Brain* online.

References

Amati-Bonneau P, Milea D, Bonneau D, Chevrollier A, Ferré M, Guillet V, et al. OPA1-associated disorders: phenotypes and pathophysiology. Int J Biochem Cell Biol 2009; 41: 1855–65.

Boldogh IR, Pon LA. Mitochondria on the move. Trends Cell Biol 2007; 17: 502–10.

Brewer GJ. Serum-free B27/neurobasal medium supports differentiated growth of neurons from the striatum, substantia nigra, septum, cerebral cortex, cerebellum, and dentate gyrus. J Neurosci Res 1995; 42: 674–83.

Chang DT, Honick AS, Reynolds IJ. Mitochondrial trafficking to synapses in cultured primary cortical neurons. J Neurosci 2006; 26: 7035–45.

Chang DT, Reynolds IJ. Differences in mitochondrial movement and morphology in young and mature primary cortical neurons in culture. Neuroscience 2006; 141: 727–36.

Chen H, Chan DC. Mitochondrial dynamics–fusion, fission, movement, and mitophagy–in neurodegenerative diseases. Hum Mol Genet 2009; 18: R169–76.

Chen H, McCaffery JM, Chan DC. Mitochondrial fusion protects against neurodegeneration in the cerebellum. Cell 2007; 130: 548–62.

Chung S, Dzeja PP, Faustino RS, Perez-Terzic C, Behfar A, Terzic A, et al. Mitochondrial oxidative metabolism is required for the cardiac differentiation of stem cells. Nat Clin Pract Cardiovasc Med 2007; 4 (Suppl 1): S60–7.

Cipolat S, Martins de Brito O, Dal Zilio B, Scorrano L. OPA1 requires mitofusin 1 to promote mitochondrial fusion. Proc Natl Acad Sci USA 2004; 101: 15927–32.

De Palma C, Falcone S, Pisoni S, Cipolat S, Panzeri C, Pambianco S, et al. Nitric oxide inhibition of Drp1-mediated mitochondrial fission is critical for myogenic differentiation. Cell Death Differ 2010; 17: 1684–96.

Delettre C, Lenaers G, Griffoin JM, Gigarel N, Lorenzo C, Belenguer P, et al. Nuclear gene OPA1, encoding a mitochondrial dynamin-related protein, is mutated in dominant optic atrophy. Nat Genet 2000; 26: 207–10.

Dickey AS, Strack S. PKA/AKAP1 and PP2A/Bbeta2 regulate neuronal morphogenesis via Drp1 phosphorylation and mitochondrial bioenergetics. J Neurosci 2011; 31: 15716–26.

Elachouri G, Vidoni S, Zanna C, Pattyn A, Boukhaddaoui H, Gaget K, et al. OPA1 links human mitochondrial genome maintenance to mtDNA replication and distribution. Genome Res 2011; 21: 12–20.

Frezza C, Cipolat S, Martins de Brito O, Micaroni M, Beznoussenko GV, Rudka T, et al. OPA1 controls apoptotic cristae remodeling independently from mitochondrial fusion. Cell 2006; 126: 177–89.

Hamanaka RB, Chandel NS. Mitochondrial reactive oxygen species regulate cellular signaling and dictate biological outcomes. Trends Biochem Sci 2010; 35: 505–13.

Ishihara N, Fujita Y, Oka T, Mihara K. Regulation of mitochondrial morphology through proteolytic cleavage of OPA1. EMBO J 2006; 25: 2966–77.

Ishihara N, Nomura M, Jofuku A, Kato H, Suzuki SO, Masuda K, et al. Mitochondrial fission factor Drp1 is essential for embryonic development and synapse formation in mice. Nat Cell Biol 2009; 11: 958–66.

Landes T, Leroy I, Bertholet A, Diot A, Khosrobakhsh F, Daloyau M, et al. OPA1 (dys)functions. Semin Cell Dev Biol 2010; 21: 593–8.

Lee SH, Kim KR, Ryu SY, Son S, Hong HS, Mook-Jung I, et al. Impaired short-term plasticity in mossy fiber synapses caused by mitochondrial dysfunction of dentate granule cells is the earliest synaptic deficit in a mouse model of Alzheimer's disease. J Neurosci 2012; 17: 5953–63.

Lenaz G, Genova ML. Structural and functional organization of the mitochondrial respiratory chain: a dynamic super-assembly. Int J Biochem Cell Biol 2009; 41: 1750–72.

Li H, Chen Y, Jones AF, Sanger RH, Collis LP, Flannery R, et al. Bcl-xL induces Drp1-dependent synapse formation in cultured hippocampal neurons. Proc Natl Acad Sci USA 2008; 105: 2169–74.

Li Z, Okamoto K, Hayashi Y, Sheng M. The importance of dendritic mitochondria in the morphogenesis and plasticity of spines and synapses. Cell 2004; 119: 873–87.

Mandal S, Lindgren AG, Srivastava AS, Clark AT, Banerjee U. Mitochondrial function controls proliferation and early differentiation potential of embryonic stem cells. Stem Cells 2011; 29: 486–95.

Masliah E, Mallory M, Alford M, DeTeresa R, Hansen LA, McKeel DW Jr, et al. Altered expression of synaptic proteins occurs early during progression of Alzheimer's disease. Neurology 2001; 56: 127–9.

Olichon A, Baricault L, Gas N, Guillou E, Valette A, Belenguer P, et al. Loss of OPA1 perturbates the mitochondrial inner membrane structure and integrity, leading to cytochrome c release and apoptosis. J Biol Chem 2003; 278: 7743–6.

Olichon A, Elachouri G, Baricault L, Delettre C, Belenguer P, Lenaers G. OPA1 alternate splicing uncouples an evolutionary conserved function in mitochondrial fusion from a vertebrate restricted function in apoptosis. Cell Death Differ 2007; 14: 682–92.

Schon EA, Przedborski S. Mitochondria: the next (neurode)generation. Neuron 2011; 70: 1033–53.

Terry RD, Masliah E, Salmon DP, Butters N, DeTeresa R, Hill R, et al. Physical basis of cognitive alterations in Alzheimer's disease: synaptic loss is the major correlate of cognitive impairment. Ann Neurol 1991; 30: 572–80.

Tsatmali M, Walcott EC, Crossin KL. Newborn neurons acquire high levels of reactive oxygen species and increased mitochondrial proteins upon differentiation from progenitors. Brain Res 2005; 1040: 137–50.

Uo T, Dworzak J, Kinoshita C, Inman DM, Kinoshita Y, Horner PJ, et al. Drp1 levels constitutively regulate mitochondrial dynamics and cell survival in cortical neurons. Exp Neurol 2009; 218: 274–85.

Verstreken P, Ly CV, Venken KJ, Koh TW, Zhou Y, Bellen HJ. Synaptic mitochondria are critical for mobilization of reserve pool vesicles at Drosophila neuromuscular junctions. Neuron 2005; 47: 365–78.

Voccoli V, Colombaioni L. Mitochondrial remodeling in differentiating neuroblasts. Brain Res 2009; 1252: 15–29.

Wang X, Su B, Lee HG, Li X, Perry G, Smith MA, et al. Impaired balance of mitochondrial fission and fusion in Alzheimer's disease. J Neurosci 2009; 29: 9090–103.

Westermann B. Mitochondrial fusion and fission in cell life and death. Nat Rev Mol Cell Biol 2010; 11: 872–84.

Westermann B. Bioenergetic role of mitochondrial fusion and fission. Biochim Biophys Acta 2012; 10: 1833–8.

Wilkerson DC, Sankar U. Mitochondria: a sulfhydryl oxidase and fission GTPase connect mitochondrial dynamics with pluripotency in embryonic stem cells. Int J Biochem Cell Biol 2011; 43: 1252–6.

Williams PA, Morgan JE, Votruba M. OPA1 deficiency in a mouse model of dominant optic atrophy leads to retinal ganglion cell dendropathy. Brain 2010; 133: 2942–51.

Williams PA, Piechota M, Von Ruhland C, Taylor E, Morgan JE, Votruba M. OPA1 is essential for retinal ganglion cell synaptic architecture and connectivity. Brain 2012; 135: 493–505.

Yu-Wai-Man P, Griffiths PG, Gorman GS, Lourenco CM, Wright AF, Auer-Grumbach M, et al. Multi-system neurological disease is common in patients with OPA1 mutations. Brain 2010; 133: 771–86.

Zhao F, Wu T, Lau A, Jiang T, Huang Z, Wang XJ, et al. Nrf2 promotes neuronal cell differentiation. Free Radic Biol Med 2009; 47: 867–79.

Zuchner S, Mersiyanova IV, Muglia M, Bissar-Tadmouri N, Rochelle J, Dadali EL, et al. Mutations in the mitochondrial GTPase mitofusin 2 cause Charcot-Marie-Tooth neuropathy type 2A. Nat Genet 2004; 36: 449–51.